

Article

A Flexible Three-in-One Microsensor for Real-Time Monitoring of Internal Temperature, Voltage and Current of Lithium Batteries

Chi-Yuan Lee ^{1,*}, Huan-Chih Peng ¹, Shuo-Jen Lee ¹, I-Ming Hung ², Chien-Te Hsieh ², Chuan-Sheng Chiou ¹, Yu-Ming Chang ¹ and Yen-Pu Huang ¹

¹ Department of Mechanical Engineering, Yuan Ze Fuel Cell Center, Yuan Ze University, Taoyuan 32003, Taiwan; E-Mails: s988705@mail.yzu.edu.tw (H.-C.P.); mesjl@saturn.yzu.edu.tw (S.-J.L.); mecschiu@saturn.yzu.edu.tw (C.-S.C.); s1005066@mail.yzu.edu.tw (Y.-M.C.); s1035061@mail.yzu.edu.tw (Y.-P.H.)

² Department of Chemical Engineering & Materials Science, Yuan Ze University, Taoyuan 32003, Taiwan; E-Mails: imhung@saturn.yzu.edu.tw (I.-M.H.); cthsieh@saturn.yzu.edu.tw (C.-T.H.)

* Author to whom correspondence should be addressed. E-Mail: cylee@saturn.yzu.edu.tw; Tel.: +886-3-4638800 (ext. 2478); Fax: +886-3-4558013.

Academic Editor: Vittorio M.N. Passaro

Received: 16 February 2015 / Accepted: 14 May 2015 / Published: 19 May 2015

Abstract: Lithium batteries are widely used in notebook computers, mobile phones, 3C electronic products, and electric vehicles. However, under a high charge/discharge rate, the internal temperature of lithium battery may rise sharply, thus causing safety problems. On the other hand, when the lithium battery is overcharged, the voltage and current may be affected, resulting in battery instability. This study applies the micro-electro-mechanical systems (MEMS) technology on a flexible substrate, and develops a flexible three-in-one microsensor that can withstand the internal harsh environment of a lithium battery and instantly measure the internal temperature, voltage and current of the battery. Then, the internal information can be fed back to the outside in advance for the purpose of safety management without damaging the lithium battery structure. The proposed flexible three-in-one microsensor should prove helpful for the improvement of lithium battery design or material development in the future.

Keywords: lithium battery; micro-electro-mechanical systems; flexible three-in-one micro- sensor; internal monitoring

1. Introduction

Many countries are devoted to alleviating global warming and finding coping strategies, especially with the development of green energy. The green energy industry includes wind power, tidal power generation, hydropower and solar power generation. These green energies use pollution-free energy sources to replace the traditional power generation systems which produce greenhouse gases. However, if these power generation systems lack a good energy storage mechanism, the excess energy will be wasted. Therefore, it is required to use energy storage devices to store the excess energy. Lithium batteries are a useful tool for energy storage.

Lithium batteries are characterized by portability, high energy density, high operating voltage, wide service temperature range, no memory effect and long life. Hence, they are indispensable energy storage devices at present. However, in the lithium battery charging/discharging process, the anode material and electrolyte perform electrochemical reactions, which generate a great deal of heat [1]. The overcharge/overdischarge can result in voltage instability and even thermal runaway [2], as well as safety problems. A new approach, suitable for real-time implementation, was introduced for estimation of the non-uniform internal temperature distribution in cylindrical lithium-ion cells, in which a radial 1-D model is used to estimate the distribution using two inputs: the real or imaginary part of the electrochemical impedance of the cell at a single frequency, and the surface temperature [3]. A preliminary calorimetric analysis and the surface temperatures of high-energy lithium-ion batteries indicated that the cells are prone to thermal runaway at temperatures of approximately 175 ~ 185 °C, which can be triggered by the Joule effect of the short circuit that results from the melting of the separator [4]. Galobardes [5] studied the application of C-MEMS as a lithium-ion battery anode. It is a protective film, referred to as a solid electrolyte interface (SEI), that forms on carbonaceous materials used as negative electrodes in commercial lithium-ion batteries. Chacko [6] studied the electrothermal model of a polymer lithium battery with LiMn_2O_4 anode material and graphite cathode material. They also conducted loop tests to draw the battery surface temperature profile models. Wiedemann [7] found that different electrolyte concentrations resulted in different voltage distributions in the lithium battery charge/discharge. Waag [8] presented a lithium battery having a large charge and discharge accelerated aging. Forgez [9] reported measurement of the internal temperature of lithium iron phosphate and coordination with a commercial thermocouple. Internal temperature measurements and surface temperature measurements of LiFePO_4 /graphite lithium-ion batteries using the model were validated in current-pulse experiments and a complete charge/discharge of the battery and were within 1.5 °C. Lee [10] developed a flexible temperature micro sensor to embed into a lithium battery. Garay [11] used MEMS techniques to develop an interdigitated electrode geometry and a minimum footprint area of 12 mm² for the medical and biological fields. Pomerantseva [12] showed that the internal stresses of battery electrodes during discharge/charge are important for improving the reliability and cycle lifetime of lithium batteries, using the stress evolution observed in a silicon

thin-film electrode incorporated into a MEMS device. Ryan [13] demonstrated thin film technologies that could produce a NiOOH cathode layer that was of high quality and only 1–5 microns thick, and demonstrated the feasibility of microscopic batteries for MEMS. Mutyala [14] used a flexible polymer produced on glass substrates and later transferred it onto thin copper foil embedded thin film thermocouples in a lithium ion battery pouch cell for *in-situ* temperature monitoring. Sun [15] reported a thermal model that can qualitatively predict the dynamic cell temperature changes that occur when a lithium ion battery works under adiabatic conditions. Richardson [16] studied a method of estimating the battery cell core and surface temperature using a thermal model coupled with electrical impedance measurements, rather than using direct surface temperature measurements. This proved advantageous compared to previous methods of estimating the temperature from impedance.

Analysis on lithium battery failure is necessary. The endogenous events of lithium batteries can be observed by real-time monitoring of the internal temperature, voltage and current of the battery, as well as by analyzing the electrochemical reactions occurring inside the battery and possible failure causes. The findings of this study can be applied to the improvement of lithium battery materials in the future, and assist lithium battery management systems to monitor the conditions and design safe failure protection early warning systems.

Existing commercial temperature, voltage and current sensors are unlikely candidates to be embedded in a lithium battery due to their large size. The probable poor airtightness of the packaging may result in electrolyte leakage, influencing the lithium battery performance and safety. The micro-electro-mechanical systems (MEMS) technology is used in this study to develop a flexible three-in-one microsensor which can be embedded in a lithium battery for real-time monitoring of the internal temperature, voltage and current. The proposed design is characterized by good accuracy, high sensitivity and short reaction times, as well as high flexibility and measurement degrees of freedom (DOF). The developed flexible three-in-one microsensor is embedded in a coin cell for real-time monitoring. The reaction inside the lithium battery can be monitored instantly and more accurately by using this method. The internal temperature uniformity and voltage and current variation are analyzed microscopically, completing the measuring tool for internal real-time microscopic monitoring and safety diagnosis of lithium batteries.

2. Theory and Design of Microsensors

The temperature microsensor used in this study was a resistance temperature detector (RTD). The sensed temperature range was wide, and the linearity was good. The serpentine sensing electrode wire of the RTD was 10 μm wide, and the interval was 10 μm . The voltage microsensor was a miniaturized voltmeter probe, and its size was 135 μm \times 100 μm . The sensing principle of the current microsensor was that the resistivity (R) of analyte and the voltage difference (V) of analyte were measured. The current value of the analyte was calculated by using Ohm's law $V = I \times R$. The current microsensor consisted of four miniature probes, including a set of two voltage measuring probes and a set of two resistance measuring probes. Their sizes were 135 μm \times 100 μm and 155 μm \times 100 μm , respectively. The structure and design of the flexible three-in-one microsensor are shown in Figure 1.

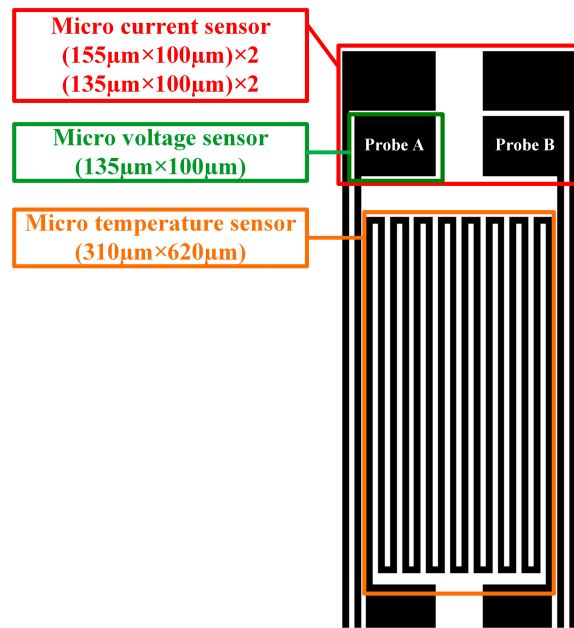


Figure 1. Structural dimensions of the flexible three-in-one microsensor.

3. Fabrication

The flexible substrate of this three-in-one microsensor was 50 μm thick polyimide (PI) foil. The foil was cleaned in acetone and methanol. An E-beam evaporator evaporated Cr (500 \AA) as adhesion layer and Au (2500 \AA) as sensing layer, as shown in Figure 2A,B. The unnecessary Au/Cr film was removed by photolithography with a wet etch to complete the microsensor layout structure, as shown in Figure 2C,D. Finally, polyimide 7505 was spin coated on the sample as insulating layer. The voltage and current probes and sensor pad end were exposed by using a photolithography process again to complete the flexible three-in-one microsensor, as shown in Figure 2E,F. The finished flexible three-in-one microsensor and an optical micrograph are shown in Figure 3.

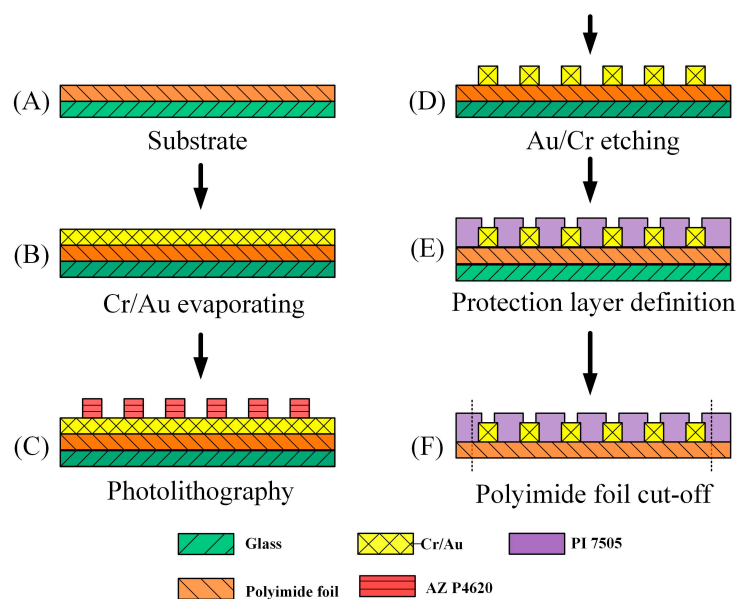


Figure 2. Production process of flexible three-in-one micro sensor.

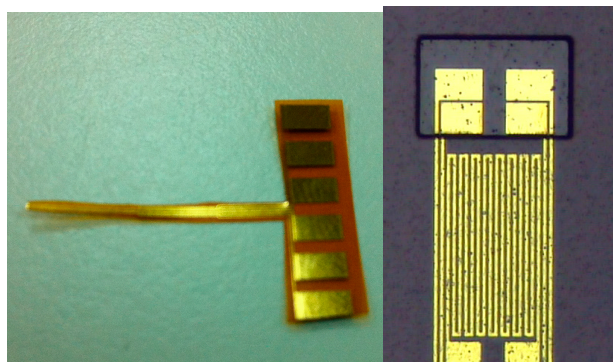


Figure 3. Finished product and optical micrograph of the flexible three-in-one microsensor.

The coin cell for this test was provided by Professor I-Ming Hung at the Department of Chemical Engineering and Materials Science (Yuan Ze University, Taoyuan, Taiwan). The cathode material was lithium titanium oxide ($\text{Li}_4\text{Ti}_5\text{O}_{12}$, LTO). The anode material was lithium iron phosphate (LFP). The lithium battery structure consisted of a top cap, anchor, current collection sheet, cathode electrode, separator, anode electrode, bottom cap and electrolyte.

The flexible three-in-one microsensors embedded in the lithium battery were numbered sensor 1 and sensor 2. Sensor 1 was embedded between the cathode electrode and separator and facing the cathode electrode. Sensor 2 was embedded between the anode electrode and separator and facing the anode electrode, as shown in Figure 4.

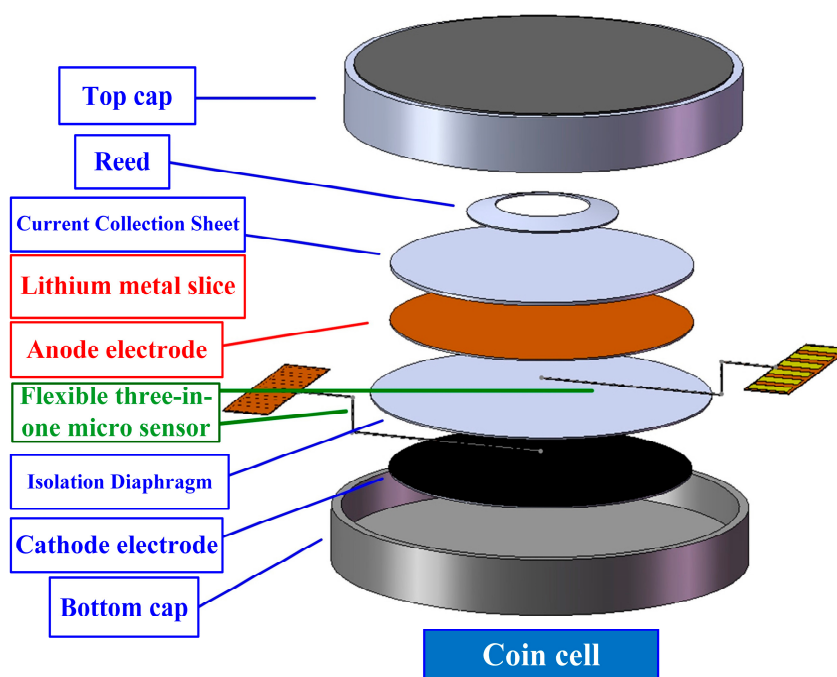


Figure 4. Schematic diagram of the package assembly of the embedded flexible three-in-one microsensors in a coin cell.

4. Coin Cell Test and Internal Real-Time Monitoring

4.1. Flexible Three-in-One Microsensor Correction

When the flexible three-in-one microsensor was completed, it was corrected to validate its reliability. After the correction procedure, a lithium battery testing machine and NI data acquisition unit were used for lithium battery tests and internal information acquisition and microscopic diagnostic analysis, to determine the differences in the electric properties of the cells with and without the flexible three-in-one microsensor. The local temperature, voltage and current changes in the lithium battery were monitored and analyzed instantly under different operating conditions. Figures 5 and 6 show the correction curves of two temperature microsensors. Each microsensor showed high linearity and high reproducibility after three correction cycles.

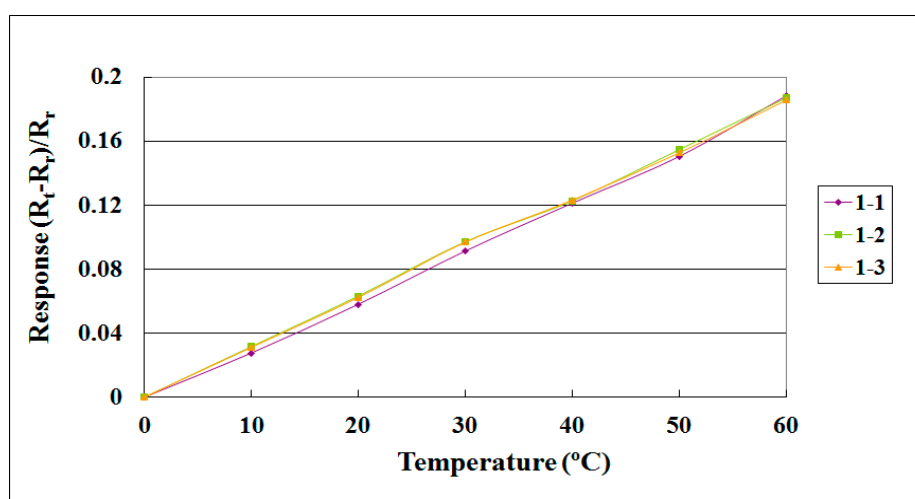


Figure 5. Correction curve of a temperature microsensor (sensor 1).

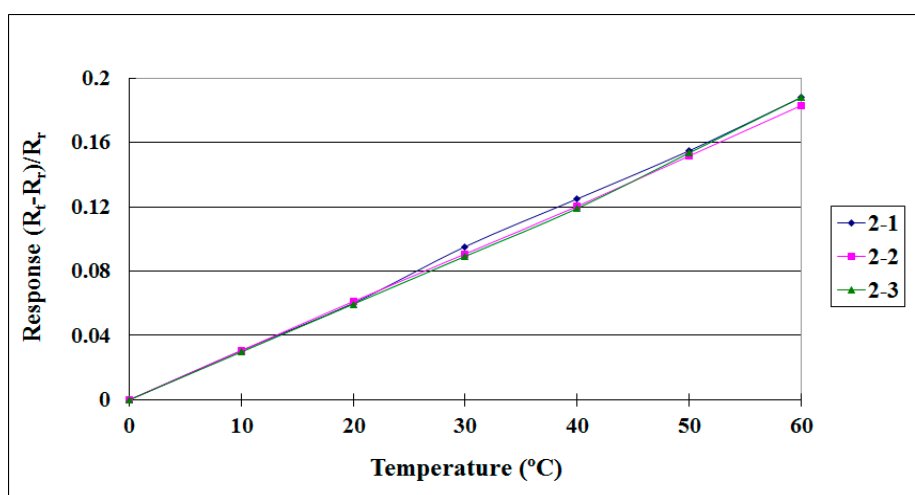


Figure 6. Correction curve of a temperature microsensor (sensor 2).

Table 1 shows the voltage correction data of the voltage microsensor. The NI measuring instrument measured the dry battery to obtain the voltage reference. The voltage microsensor then measured the dry battery. The correction difference was obtained by subtracting the voltage measured by the voltage

microsensor from the dry battery voltage. It was observed that the voltage error in the voltage measurements resulting from the voltage microsensor conductor was 0.001 V ~ 0.006 V, and the influence was low.

Table 1. Correction data of micro voltage sensor.

Sensor	Voltage Correction		Percentage to Total	
	Difference (mV)		Voltage (%)	
	Probe A	Probe B	Probe A	Probe B
Sensor 1	9.2998	9.2997	0.000001	0.000003
Sensor 2	9.2996	9.2999	0.000002	0.000001

The current microsensor was corrected by using a standard electrical conductivity solution as reference. The resistivity in the solution was measured by using the current microsensor and converted into electrical conductivity, and compared with the theoretical value of a standard electrical conductivity solution for confirming the reliability of the current microsensor. Table 2 compares the resistivity of the standard electrical conductivity solution measured by the current microsensor with the theoretical value. It was observed that the difference between measured value and theoretical value was less than 1%.

Table 2. Comparison between measured value and theoretical value of electrical conductivity.

Sensor	Theoretical Value (μScm^{-1})	Measured Value (μScm^{-1})	Percentage of Difference (%)
Sensor 1	1412	1401	0.78
Sensor 2	1412	1403	0.64

4.2. Coin Cell Test

The electrochemical performance of Li-ion batteries was tested using CR2032-type coin cells. The cathode (LiFePO_4) and anode ($\text{Li}_4\text{Ti}_5\text{O}_{12}$) powders were mixed with a binder (polyvinylidene fluoride) and two conducting media (Super-P and KS-4) at a weight ratio of 80:10:5:5 in *N*-methylpyrrolidinone (NMP) solvent to form the electrode slurry. The mixture was blended by a three-dimensional mixer using Zr balls for 3 h to prepare a uniform slurry. Then, the resultant slurry was uniformly pasted on Al (for cathode) and Cu (for anode) foil substrates with a doctor blade, followed by evaporation of the NMP solvent with a blow dryer. The prepared cathode sheets were dried at 135 °C in a vacuum oven for 12 h and pressed under a pressure of approximately 200 kg·cm⁻². The electrode layers were adjusted to a thickness of ~100 μm. The coin cells were assembled in a glove box for their electrochemical characterization, using an electrochemical analyzer (CHI 608, CH Instruments, Inc., Austin, TX, USA). In the test cells, the Li foil and the porous polypropylene film served as the counter electrode and the separator, respectively. The electrolyte solution was 1.0 M LiPF_6 in a mixture of ethylene carbonate, polycarbonate, and dimethyl carbonate with a weight ratio of 1:1:1. The charge/discharge cycling tests at different C rates (from 0.1 to 10 C) were performed within the voltage region at ambient temperature.

The lithium battery charging/discharging set CHG-5500C was used in this study for testing the coin cell. The coin cell embedded with flexible three-in-one microsensors was placed on the test carrier. A thermocouple temperature recorder was placed on the lithium battery surface to measure and record the battery surface temperature instantly. The NI Data Acquisition System performed real-time measurements and data acquisition of the flexible three-in-one microsensor. Figure 7 shows the coin cell assembly and instrument mounting. The lithium battery was embedded with two flexible three-in-one microsensors.

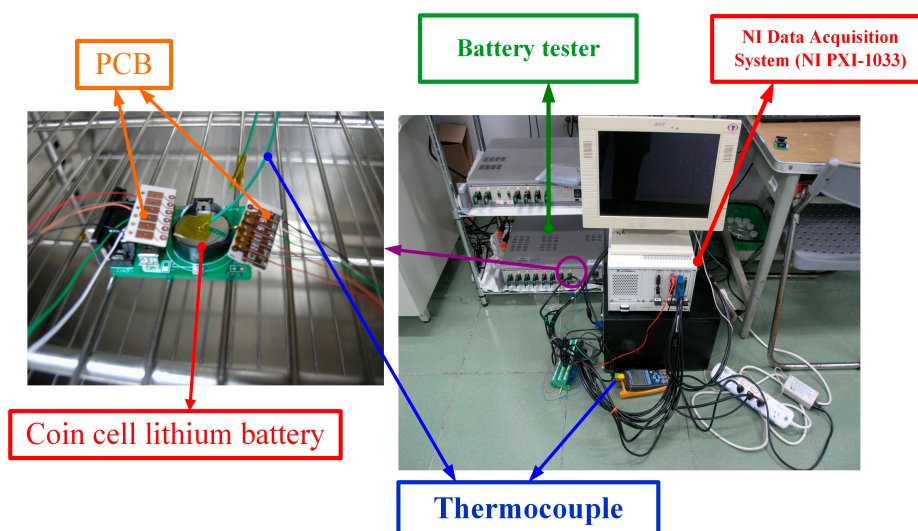


Figure 7. Coin cell test assembly and instrument mounting.

The anode material of the coin cell was LFP, the cathode material was LTO, and the theoretical capacitance value was $170 \text{ mA}\cdot\text{h}\cdot\text{g}^{-1}$. The test conditions included constant current (CC), charging/discharging voltage range $0.5 \sim 2.9 \text{ V}$. The six charge/discharge rates, ranging from 0.1 to 10 C, are frequently used for evaluating the performance of Li-ion batteries. The performance of Li-ion batteries charged at 0.1–0.5 C reflects the capability for general 3 C portable electronics, whereas the charge-discharge curves at $>2 \text{ C}$ could serve as a crucial index for evaluating the cell performance for EVs and mobile tools. Nominal capacity ($120 \text{ mA}\cdot\text{h}\cdot\text{g}^{-1}$ for LiFePO_4 cathode), separator (Celgard), maximal charge/discharge rate (10 C), and operating potential range ($0.5\sim 3.0 \text{ V}$). The test process is shown in Table 3.

Table 3. Coin cell test process (three cycles at each C-rate).

C-Rate	Charge		Discharge	
	Trigger Voltage	Static Voltage	Trigger Voltage	Static Voltage
0.1 C	0.5 V	2.9 V	2.9 V	0.5 V
0.2 C	0.5 V	2.9 V	2.9 V	0.5 V
0.5 C	0.5 V	2.9 V	2.9 V	0.5 V
1 C	0.5 V	2.9 V	2.9 V	0.5 V
5 C	0.5 V	2.9 V	2.9 V	0.5 V
10 C	0.5 V	2.9 V	2.9 V	0.5 V

Figure 8 is the charge-discharge test curve diagram of the coin cell embedded with three-in-one microsensors. The maximum unit cumulative capacity of the 0.1 C charge-discharge test was $92.4731 \text{ mA}\cdot\text{h}\cdot\text{g}^{-1}$, and the maximum unit cumulative capacity of 0.1 C discharge test was $61.7204 \text{ mA}\cdot\text{h}\cdot\text{g}^{-1}$. The calculated irreversible capacity was $30.7527 \text{ mA}\cdot\text{h}\cdot\text{g}^{-1}$, accounting for about 33.26% of the initial value.

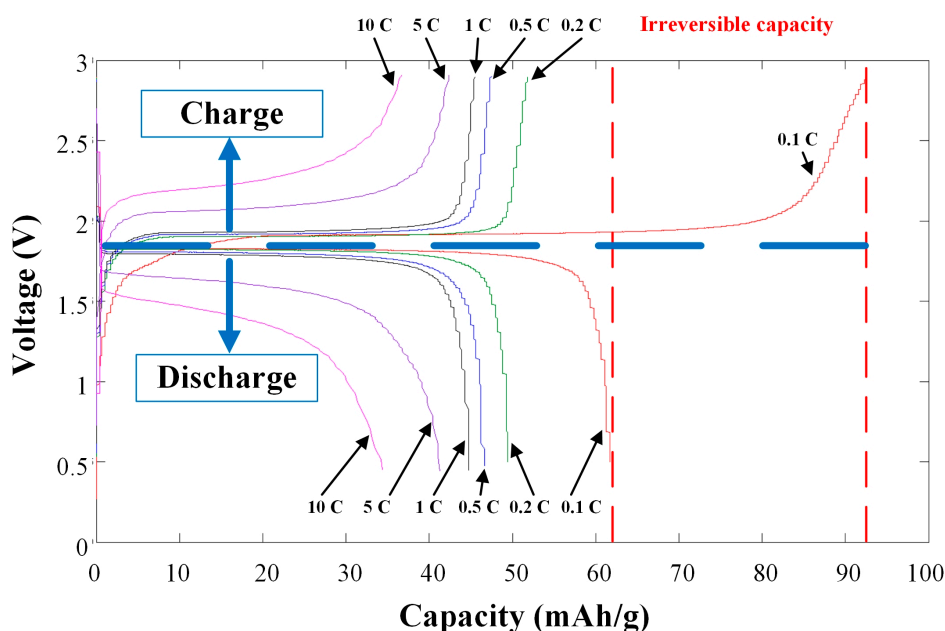


Figure 8. Charge-discharge test curve diagram of the coin cell embedded with flexible three-in-one microsensors.

Table 4 shows the maximum unit cumulative capacity of charge and discharge of coin cell at various C-rates. Figure 9, Table 5, Figure 10 and Table 6 show the maximum unit cumulative capacity in various cycles of coin cell charge/discharge tests. The electrical performance of the lithium battery in maximum unit cumulative capacity was not good. In the 5 C charge-discharge test, the residual capacity still accounted for 45.81% of the initial value, and even for 39.77% of the initial value in the 10 C charge-discharge test. The lithium battery charge/discharge test did not have complete failure in the end and the lithium battery could complete the overall charge-discharge test process.

Table 4. Comparison of maximum unit cumulative capacity of coin cell charge and discharge at various C-rates.

C-Rate	Maximum Unit Cumulative Capacity ($\text{mA}\cdot\text{h}\cdot\text{g}^{-1}$)	
	Charge	Discharge
0.1 C	92.4731	61.7204
0.2 C	51.8280	49.4624
0.5 C	47.5269	46.6667
1 C	45.5914	44.7311
5 C	42.3656	41.2903
10 C	36.7742	34.4086

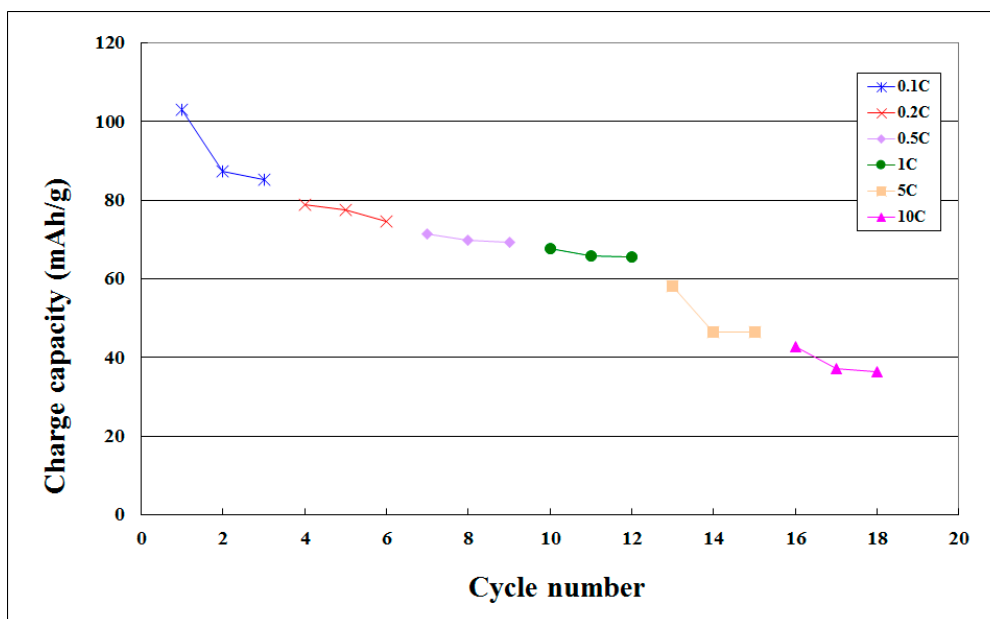


Figure 9. Maximum unit cumulative capacity curve in various cycles of coin cell charge tests.

Table 5. Maximum unit cumulative capacity in various cycles of coin cell charge tests.

C-Rate	Cycle Number	Charge Capacity (mAh/g)
0.1 C	1	103.117
	2	82.2727
	3	85.1948
0.2 C	4	78.961
	5	77.4026
	6	74.5455
0.5 C	7	71.4286
	8	69.8701
	9	69.3506
1 C	10	67.7922
	11	65.7143
	12	65.4545
5 C	13	58.1818
	14	46.4935
	15	46.4935
10 C	16	42.8571
	17	37.1429
	18	36.3636

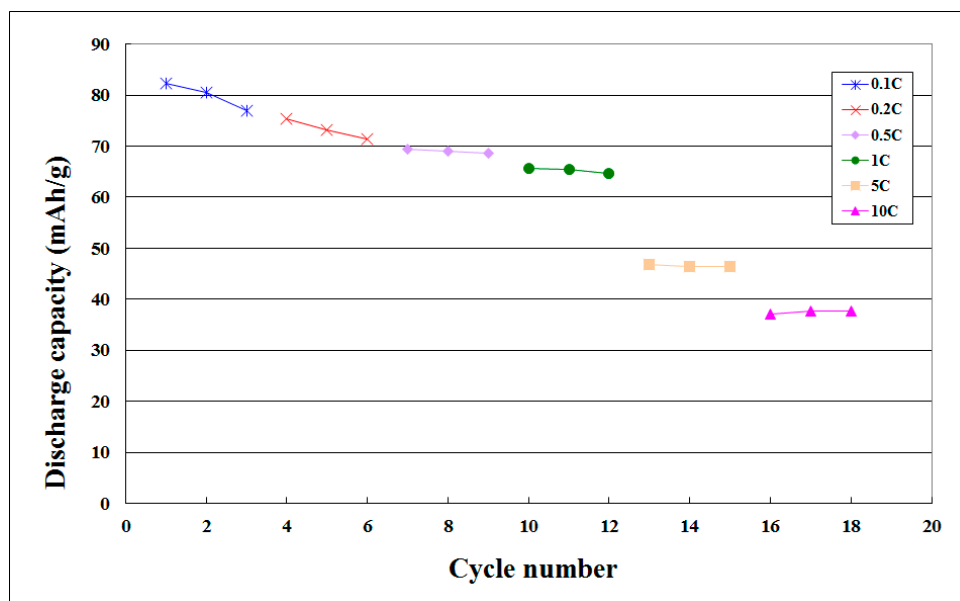


Figure 10. Maximum unit cumulative capacity curve in various cycles of coin cell discharge tests.

Table 6. Maximum unit cumulative capacity in various cycles of coin cell discharge tests.

C-Rate	Cycle Number	Discharge Capacity (mA·h/g)
0.1 C	1	82.3377
	2	80.5195
	3	76.8831
0.2 C	4	75.3247
	5	73.2468
	6	71.4286
0.5 C	7	69.3506
	8	69.0909
	9	68.5714
1 C	10	65.7143
	11	65.4545
	12	64.6753
5 C	13	46.7532
	14	46.4935
	15	46.4935
10 C	16	37.6623
	17	37.6623
	18	37.142

Table 7 shows the performance of the lithium batteries with and without the three-in-one microsensors. The maximum performance difference between the lithium batteries with and without the three-in-one microsensors was only about 10.32%. CA ratio is the weight ratio of anode and cathode materials. In the operation of lithium batteries, the cathode releases lithium ions, and the anode receives the lithium ions. When the releasing capacity of cathode was higher than the receptivity of the anode, the lithium ions could not be received by the anode completely in discharge, so the

maximum capacitance value could not be reached. If the releasing capacity of the cathode was lower than the receptivity of the anode, the anode could not release lithium ions completely to the cathode during charge. The lithium battery performance was thus influenced. The difference between CA ratios with and without three-in-one micro sensor was 8.64%. Disregarding this factor, the influence of the three-in-one microsensor on the lithium battery performance was 1.68%. Therefore, the flexible three-in-one microsensor embedded in the lithium battery for real-time measurement had only a slight influence on the electrical performance of the battery. Basically, the specific capacity as a decreasing function of C rate can be attributed to a polarization situation, indicating poor electronic conductivity and slow ionic diffusion rate. On the basis of the experimental results, the degradation of specific capacity at high C rates is minor, e.g., the capacity retention still remains at >60 for the ratio of specific capacity at 0.1 C to 5 C.

Table 7. Comparison of performance of lithium batteries with and without embedded three-in-one microsensors.

		With Microsensor	Without Microsensor	Difference Ratio
Maximum cumulative unit capacity (mA·h·g ⁻¹)	Charge	92.4731	103.1169	10.32%
	Discharge	61.7204	68.5741	9.99%

4.3. Persistence Effect Test for the Flexible Three-in-One Microsensors

The total time for the lithium battery charge/discharge test was about 109.8 h, 0.1 C accounted for 60 h, 0.2 C accounted for 30 h, 0.5 C accounted for 12 h, 1 C accounted for 6 h, 5 C accounted for 1.2 h and 10 C accounted for 0.6 h. The monitoring data are shown in Table 8. After the coin cell charge-discharge test, the flexible three-in-one microsensor performed temperature correction again, as shown in Figure 11. The correction curve still showed high linearity, suggesting that the flexible three-in-one microsensor is durable and reliable.

Table 8. Internal monitoring data of the persistence effect test for lithium battery charge/discharge.

SENSOR No.	Internal-External Temperature Difference (°C)		Voltage Difference (V)		Current (mA)	
	1	2	1	2	1	2
0.1 C	0.55	0.56	0.1306	0.0750	0.169	0.170
0.2 C	0.78	0.76	0.1260	0.0714	0.172	0.171
0.5 C	0.85	0.86	0.1301	0.0660	0.184	0.173
1 C	0.97	0.98	0.1312	0.0690	0.186	0.184
5 C	0.60	0.65	0.1276	0.0760	0.193	0.190
10 C	0.45	0.30	0.1351	0.0790	0.199	0.199

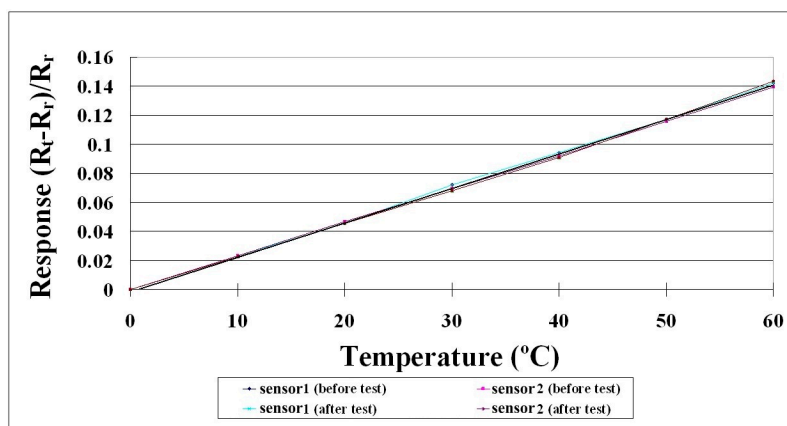


Figure 11. Microsensor temperature correction curve before and after coin cell charge-discharge tests.

5. Conclusions

The flexible micro temperature-voltage-current sensor was successfully integrated into PI by using MEMS technology in this study. The total thickness of three-in-one microsensor was 58 μm . It is characterized by quick response, real-time measurement and good durability.

After the temperature, voltage and electrical conductivity correction of the flexible microsensor, the temperature correction curve shows high linearity and good reproducibility. The voltage and electrical conductivity correction shows the error value of microsensor measurement is smaller than 1%, proving the reliability of the flexible microsensor in temperature, voltage and current measurements. The flexible three-in-one microsensor was successfully embedded in a coin cell in this study. According to the performance of the batteries with and without three-in-one microsensors, the three-in-one micro-sensor could measure the internal temperature, voltage and current of coin cell instantly without disturbing the operation of the lithium battery.

Acknowledgements

This work was accomplished with much needed support and the authors would like to thank for the financial support by Ministry of Science and Technology of R.O.C. through the grant MOST 99-2632-E-155-001-MY3, 102-2221-E-155-033-MY3 and 104-2622-E-155-004. In addition, we would like to thank the YZU NENS Common Lab for providing access to their research facilities.

Author Contributions

The work presented here was carried out in collaboration between all authors. Chi-Yuan Lee, Shuo-Jen Lee, I-Ming Hung, Chien-Te Hsieh, and Chuan-Sheng Chiou conceived, designed and discussed this study. Huan-Chih Peng, Yu-Ming Chang and Yen-Pu Huang performed the experiments and analyzed the data. All authors have contributed, reviewed and improved the manuscript.

Conflicts of Interest

The authors declare no conflict of interest.

References

1. Baba, Y.; Okada, S.; Yamaki, J. A breakthrough in the safety of lithium secondary batteries by coating the cathode material with AlPO_4 nanoparticles. *Solid State Ion.* **2002**, *148*, 311–316.
2. Wang, Q.; Ping, P.; Zhao, X.; Chu, G.; Sun, J.; Chen, C. Thermal runaway caused fire and explosion of lithium ion battery. *J. Power Sources* **2012**, *208*, 210–224.
3. Richardson, R.R.; Ireland, P.T.; Howey, D.A. Battery internal temperature estimation by combined impedance and surface temperature measurement. *J. Power Sources* **2014**, *265*, 254–261.
4. Ping, P.; Wang, Q.S.; Huang, P.F.; Li, K.; Sun, J.H.; Kong, D.P.; Chen, C.H. Study of the fire behavior of high-energy lithium-ion batteries with full-scale burning test. *J. Power Sources* **2015**, *285*, 80–89.
5. Galobardes, F.; Wang, C.; Madou, M. Investigation on the solid electrolyte interface formed on pyrolyzed photoresist carbon anodes for C-MEMS lithium-ion batteries. *Diam. Relat. Mater.* **2006**, *15*, 1930–1934.
6. Chacko, S.; Chung, Y.M. Thermal modelling of Li-ion polymer battery for electric vehicle drive cycles. *J. Power Sources* **2012**, *213*, 296–303.
7. Wiedemann, A.H.; Goldin, G.M.; Barnett, S.A.; Zhu, H.; Kee, R.J. Effects of three-dimensional cathode microstructure on the performance of lithium-ion battery cathodes. *Electrochim. Acta* **2013**, *88*, 580–588.
8. Waag, W.; Kbäitz, S.; Sauer, D.U. Experimental investigation of the lithium-ion battery impedance characteristic at various conditions and aging states and its influence on the application. *Appl. Energy* **2013**, *102*, 885–897.
9. Forgez, C.; Do, D.V.; Friedrich, G.; Morcrette, M.; Delacourt, C. Thermal modeling of a cylindrical LiFePO_4 /graphite lithium-ion battery. *J. Power Sources* **2010**, *195*, 2961–2968.
10. Lee, C.Y.; Lee, S.J.; Tang, M.S.; Chen, P.C. *In situ* monitoring of temperature inside lithium-ion batteries by flexible micro temperature sensors. *Sensors* **2011**, *11*, 9942–9950.
11. Garay, E.F.; Bashirullah, R. Biofluid activated microbattery for disposable microsystems. *J. Microelectromech. Syst.* **2015**, *24*, 70–79.
12. Pomerantseva, E.; Jung, H.; Gnerlich, M.; Baron, S.; Gerasopoulos, K.; Ghodssi, R. A MEMS platform for *in situ*, real-time monitoring of electrochemically induced mechanical changes in lithium-ion battery electrodes. *J. Micromech. Microeng.* **2013**, *23*, doi:10.1088/0960-1317/23/11/114018.
13. Ryan, D.M.; Rodney, M.L.; Linton, S. Microscopic batteries for micro electromechanical systems (MEMS). In Proceedings of the 32nd Intersociety Energy Conversion Engineering Conference, Honolulu, HI, USA, 27 July–1 August 1997; pp. 77–82.
14. Mutyala, M.; Santosh, K.; Zhao, J.; Li, J.; Pan, H.; Yuan, C.; Li, X. *In-situ* temperature measurement in lithium ion battery by transferable flexible thin film thermocouples. *J. Power Sources* **2014**, *260*, 43–49.
15. Sun, Q.; Wang, Q.; Zhao, X.; Sun, J.; Lin, Z. Numerical study on lithium titanate battery thermal response under adiabatic condition. *Energy Convers. Manag.* **2015**, *92*, 184–193.
16. Richardson, R.R.; Howey, D.A. Sensorless battery internal temperature estimation using a kalman filter with impedance measurement. *IEEE Trans. Sustain. Energy* **2015**, in press.